Cancelable fusion-based face recognition

Article *in* Multimedia Tools and Applications · November 2019

DOI: 10.1007/s11042-019-07848-y

Multimedia Tools and Applications
https://doi.org/10.1007/s11042-019-07848-y

Cancelable fusion-based face recognition

Essam Abdellatef[1] · Nabil A. Ismail[2] · Salah Eldin S. E. Abd Elrahman[2] · Khalid N. Ismail[3,4] · Mohamed Rihan[5] · Fathi E. Abd El-Samie[5]

Received: 14 September 2018 / Revised: 15 May 2019 / Accepted: 31 May 2019
Published online: 23 July 2019

Abstract
Biometric recognition refers to the automated process of recognizing individuals using their biometric patterns. Recent advancements in deep learning and computer vision indicate that generic descriptors which are extracted using convolutional neural networks (CNNs) could represent complex image characteristics. This paper presents a number of cancelable fusion-based face recognition (FR) methods; region-based, multi-biometric and hybrid-features. The former included methods incorporate the use of CNNs to extract deep features (DFs). A fusion network combines the DFs to obtain a discriminative facial descriptor. Cancelabilitiy is provided using bioconvolving as an encryption method. In the region-based method, the DFs are extracted from different face regions. The multi-biometric method uses different biometric traits to train multiple CNNs. The hybrid-features method merges the merits of deep-learned features and hand-crafted features to obtain a more representative output. Also, an efficient CNN model is proposed. Experimental results on various datasets prove that; (a) the proposed CNN model achieves remarkable results compared to other state-of-the-art CNNs, (b) region-based method is superior to multi-biometric and hybrid-features methods and (c) the utilization of bio-convolving method increases the system security with a slight degradation in the recognition accuracy.

Keywords Deep features, Fusion network, and cancelable biometrics

1 Introduction

In recent years, FR is considered as a promising option for human individuals' identification due to the wide improvement and adoption of digital photography. People can access their accounts by using secret codes that are constructed from numbers and alphabets. These codes are unique, but at the same time they could be stolen by criminals or forgotten by users [1, 20, 36].

Users could be identified by face, iris, fingerprint, blood, or DNA. FR is preferable for users as it does not require active co-operation of a person. Besides, FR does not require multiple distributed

✉ Essam Abdellatef
essam_abdellatef@yahoo.com

Extended author information available on the last page of the article

cameras as in body texture identification or high-precision sensors as in iris and fingerprint recognition. FR is concerned with the appearance association of faces with the corresponding identities through: (a) an identification scenario that is used for identity prediction of a face image and (b) a verification scenario that determines whether a pair of images shares the same identity or not [14, 35].

There are several FR technical trends such as holistic learning, local hand-crafted feature extraction, shallow learning, and deep learning (DL). In holistic learning, a sparse representation [52] or manifold [17] is used to derive the low-dimensional representations. These methods could not help in dealing with the uncontrolled facial changes. In local hand-crafted feature extraction,

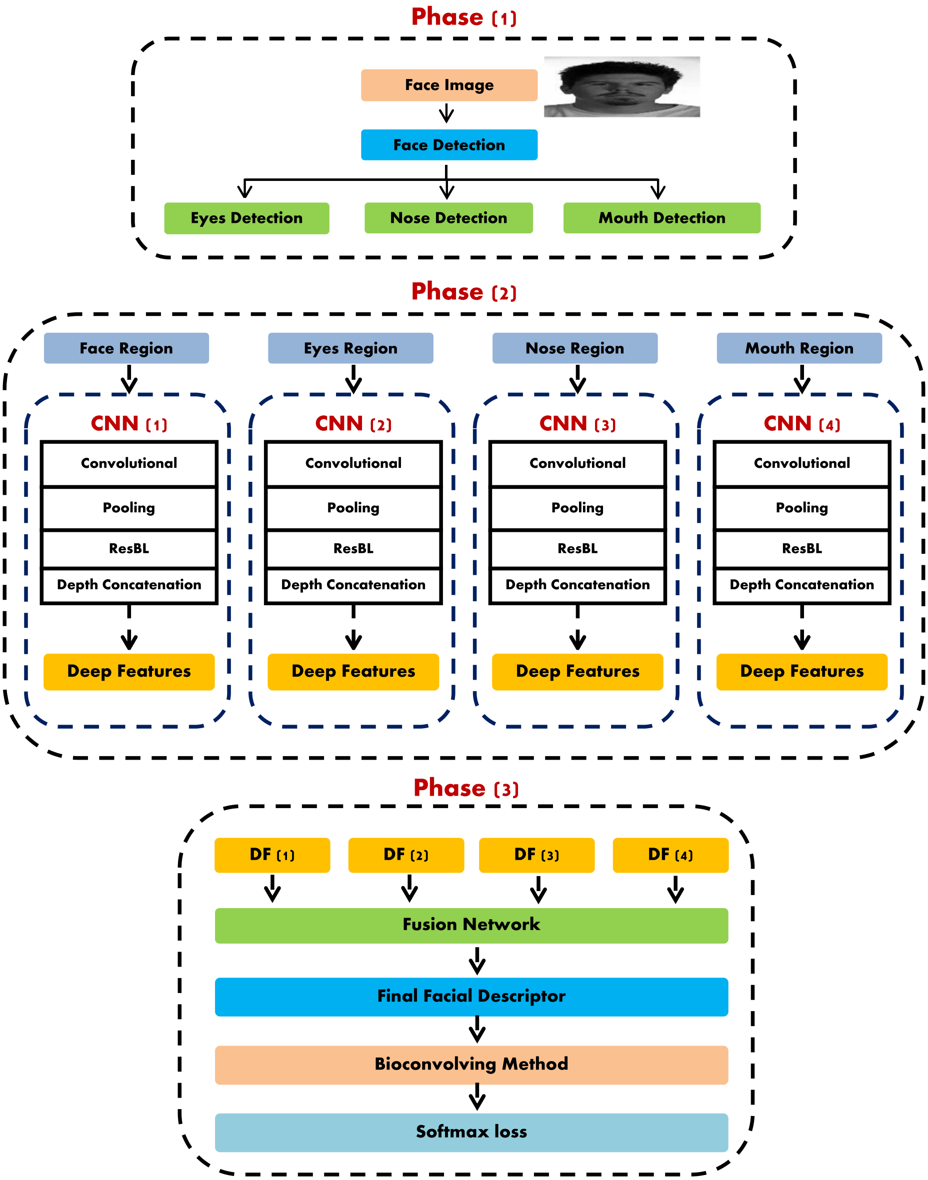

Fig. 1 Flowchart of region-based FR

well-known algorithms are used to extract features from face images. This approach achieves a promising performance using invariant local filtering properties. On the other hand, performance degradation could occur due to the lack of compactness and distinctiveness. In shallow learning, the compactness issue can be solved by learning the encoding codebook. However, this approach suffers from robustness limitations due to the complex appearance variations of facial images. In DL, feature extraction and transformation are performed using multiple layers of processing units. Moreover, DL learns multiple levels of representations including invariance of facial expressions, pose and lighting. Convolutional neural network (CNN) is the most popular deep learning model used in FR. The first layer in a CNN is similar to the Gabor filter, while the other layers extract more complex patterns such as high-bridged nose, eye color and smile. In 2014, an improvement in recognition accuracy (97.35%) has been achieved using DeepFace [48] on the LFW benchmark. We can say that DL reshapes the FR research landscape with respect to datasets and evaluation protocols.

The increasing demand for providing security and privacy of biometric templates raises more challenges for FR systems. Thanks to cancelable biometric techniques [34, 39, 49], biometric data

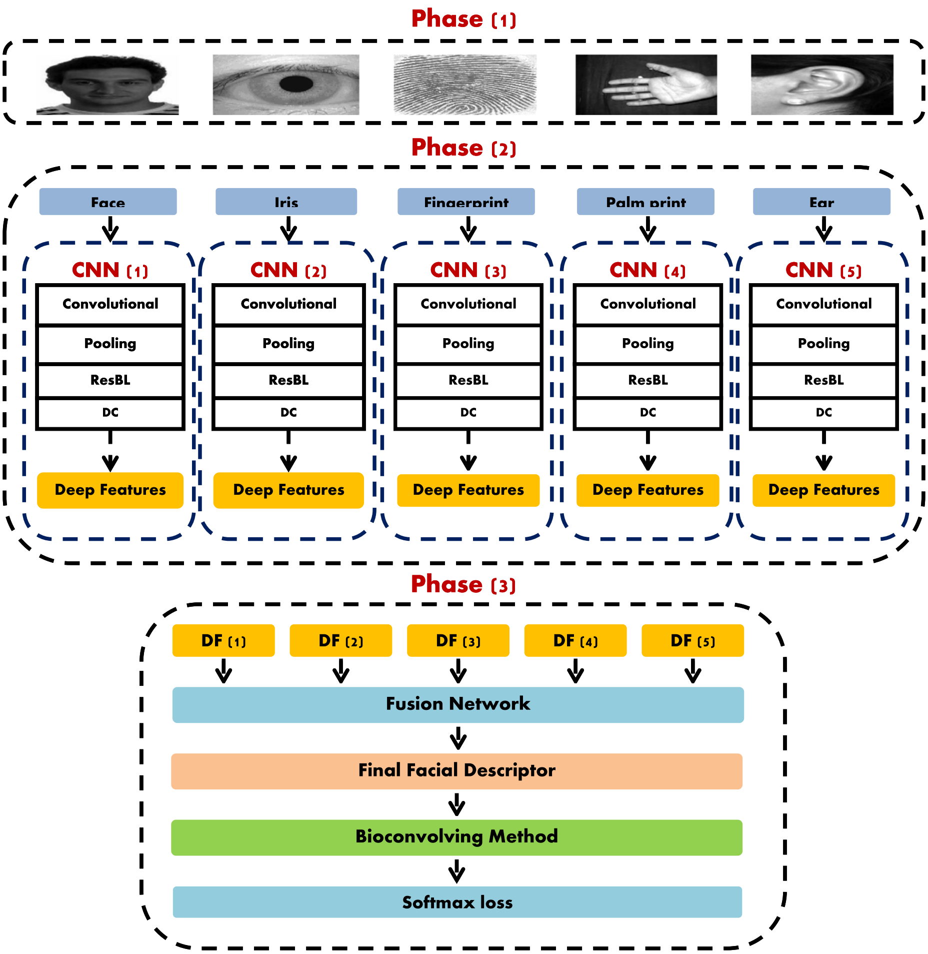

Fig. 2 Flowchart of multi-biometric FR method

protection can be provided without degradation in the system performance. In this paper, some cancelable FR methods are introduced. The proposed methods use CNNs to extract DFs from face images. A fusion network combines features to obtain a more representative facial descriptor. Finally, bioconvolving method is applied to provide revocability and privacy of the biometric data. Furthermore, an efficient CNN model is presented.

The main contributions of this work are;

- Proposal of a new CNN model to extract more robust and reliable DFs.
- In-depth analysis of the proposed cancelable FR methods.

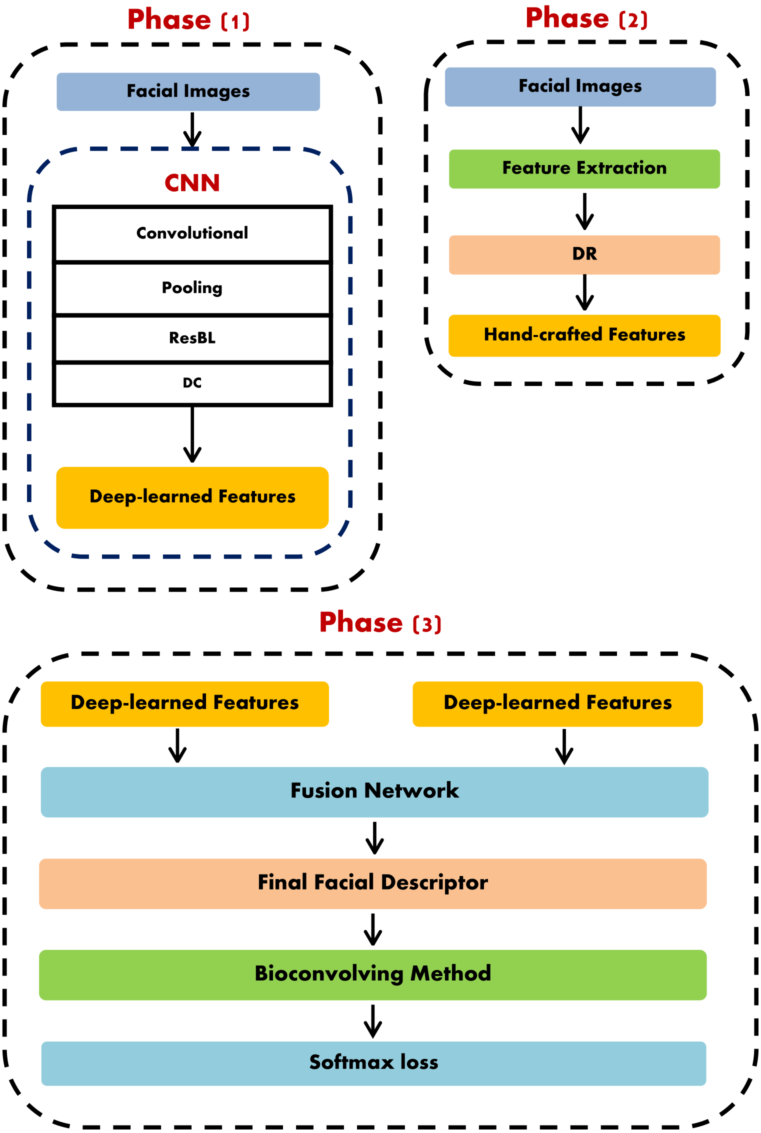

Fig. 3 Flowchart of the hybrid-features FR method

Table 1 Phases of the proposed FR methods

Phases	Region-based	Multi-biometric	Hybrid-features
Phase (1)	A face detection process [27] is applied on the original images to obtain face regions. Then, eyes, nose and mouth detection operations are performed to detect eyes, nose and mouth regions, respectively.	Data collection is performed for different biometric traits: face, iris, fingerprint, palm print and ear.	CNN is used to extract DFs from images.
Phase (2)	Four CNNs extract DFs from the detected regions.	Features are extracted using CNNs from biometric templates.	Hand-crafted features are extracted using traditional algorithms. Additionally, a data reduction (DR) method is used to reduce the dimensions of these features to be consistent with the dimensions of deep-learned ones.
Phase (3)	A fusion network combines features to form the final facial descriptor, and then bioconvolving method is applied.		

Table 2 Essential rules of CNN layers

CNN Layers	Essential rule
Convolutional	Use of a number of learnable filters to compute dot products between the entries of both filter and input image. The output feature map $f^{C,l}_{x,y,k}$ for a particular layer l and an input $f^{O_p,l-1}_{x,y}$, can be computed as: $$f^{C,l}_{x,y,k} = {w^l_k}^T f^{O_p,l-1}_{x,y} + b^l_k \quad (1)$$ where w^l_k is the shared weights, b^l_k is the bias and C denotes convolution. O_p represents the input image, for $l = 1$, while it represents convolution, pooling or activation, for $l > 1$.
Max Pooling	Computing the maximum value in a local spatial neighborhood and then spatial resolution is reduced: $$f^{P,l}_{x,y,k} = \max_{(m,n)\in N_{x,y}} f^{Op,l-1}_{m,n,k} \quad (2)$$ where the pooling operation is denoted by P and the local spatial neighborhood of *(x, y)* coordinate is denoted by $N_{x,\ y}$.
Batch Normalization	Normalization of the activations of the previous layer, training the network faster, making weights easier to be initialized and simplifying the creation of deeper networks.
Residual Learning Block "ResBL"	Optimization of the loss of CNNs in an easy way. The output of a residual block R can be expressed as: $$f^{R,l}_{x,y,k} = f^{Op,l-q}_{x,y} + F\left(f^{Op,l-q}_{x,y}, \{W_k\}\right) \quad (3)$$ where $f^{Op,l-q}_{x,y}$ is the input feature map, $F(.)$ is the residual mapping to be learned and q is the total number of stacked layers.
Depth Concatenation	Increasing the depth of the feature map by concatenating the output filter banks of a number of layers into a single output vector.
Feature Normalization	Ensuring that all features have equal contribution to the cost function. Normalized features $f^{N_r}_i$ to the softmax loss will be provided as $f^{N_r} = \frac{f^{Op}-\mu}{\sqrt{\sigma^2}}$, where μ and σ^2 represent the mean and variance, respectively.
Softmax Loss	Computing the loss. The form of computing softmax loss is: $$L_{softmax} = -\sum_{i=1}^{N} \log \frac{e^{\mathbf{w}^T_{y_i}\mathbf{f}_i + b_{y_i}}}{\sum_{j=1}^{K} e^{\mathbf{w}^T_j \mathbf{f}_i + b_j}} \quad (4)$$ where f_i denotes the features and y_i is the true class label of the i^{th} image. w_j and b_j are the weights and bias of the j^{th} class, respectively. N is the number of training samples and K is the number of classes.

Table 3 The proposed CNN model

Layer Name	No. of Filters	Filter Size	Stride Size	Padding Size
Conv1	64	7 × 7 × 3	2 × 2	3 × 3
ReLU	n/a	n/a	n/a	n/a
Max Pooling	1	3 × 3	2 × 2	1 × 1
Batch Normalization	Batch Normalization			
Conv2	64	1 × 1 × 64	1 × 1	0
ReLU	n/a	n/a	n/a	n/a
Conv3	128	3 × 3 × 64	1 × 1	1 × 1
ReLU	n/a	n/a	n/a	n/a
Max Pooling	1	3 × 3	2 × 2	1 × 1
ResBL	1	3 × 3 × 64	1 × 1	1 × 1
Conv4	192	3 × 3 × 64	1 × 1	1 × 1
ReLU	n/a	n/a	n/a	n/a
Max Pooling	1	3 × 3	1 × 1	1 × 1
ResBL	1	3 × 3 × 64	1 × 1	1 × 1
Conv5	64	1 × 1 × 192	1 × 1	0
ReLU	n/a	n/a	n/a	n/a
Conv6	96	1 × 1 × 192	1 × 1	0
ReLU	n/a	n/a	n/a	n/a
Conv7	128	3 × 3 × 96	1 × 1	1 × 1
ReLU	n/a	n/a	n/a	n/a
Conv8	16	1 × 1 × 192	1 × 1	0
ReLU	n/a	n/a	n/a	n/a
Conv9	32	5 × 5 × 16	1 × 1	2 × 2
ReLU	n/a	n/a	n/a	n/a
Max Pooling	1	3 × 3	1 × 1	1 × 1
Conv10	32	1 × 1 × 192	1 × 1	0
ReLU	n/a	n/a	n/a	n/a
Depth Concatenation	Depth Concatenation of 4 Inputs			
Conv11	128	1 × 1 × 256	1 × 1	0
ReLU	n/a	n/a	n/a	n/a
Conv12	128	1 × 1 × 256	1 × 1	0
ReLU	n/a	n/a	n/a	n/a
Conv13	192	3 × 3 × 128	1 × 1	1 × 1
ReLU	n/a	n/a	n/a	n/a
Conv14	32	1 × 1 × 256	1 × 1	0
ReLU	n/a	n/a	n/a	n/a
Conv15	96	5 × 5 × 32	1 × 1	2 × 2
ReLU	n/a	n/a	n/a	n/a
Max Pooling	1	3 × 3	1 × 1	1 × 1
Conv16	64	1 × 1 × 256	1 × 1	0
ReLU	n/a	n/a	n/a	n/a
Depth Concatenation	Depth Concatenation of 4 Inputs			
Conv17	192	1 × 1 × 480	1 × 1	0
ReLU	n/a	n/a	n/a	n/a
Conv18	96	1 × 1 × 480	1 × 1	0
ReLU	n/a	n/a	n/a	n/a
Conv19	208	3 × 3 × 96	1 × 1	1 × 1
ReLU	n/a	n/a	n/a	n/a
Conv20	16	1 × 1 × 480	1 × 1	0
ReLU	n/a	n/a	n/a	n/a
Conv21	48	5 × 5 × 16	1 × 1	2 × 2
ReLU	n/a	n/a	n/a	n/a
Max Pooling	1	3 × 3	1 × 1	1 × 1
Conv22	64	1 × 1 × 480	1 × 1	0
ReLU	n/a	n/a	n/a	n/a
Depth Concatenation	Depth Concatenation of 4 Inputs			

Table 3 (continued)

Layer Name	No. of Filters	Filter Size	Stride Size	Padding Size
Max Pooling	1	3 × 3	2 × 2	0
Dropout	40% Dropout			
Fully Connected Layer	1000 Fully Connected Layer			
Feature Normalization	Feature Normalization			
Softmax	n/a	n/a	n/a	n/a

Table 4 Performance metrics equations

Performance Metric	Equation
Accuracy	$\frac{TP+TN}{TP+FP+FN+TN}$
Specificity	$\frac{TN}{FP+TN}$
Precision	$\frac{TP}{TP+FP}$
Recall	$\frac{TP}{TP+FN}$
F_{score}	$\frac{2*Recall*Precision}{Recall+Precision}$

TP = True Positive, FN = False Negative, FP = False Positive, and TN = True Negative.

- Extensive experiments on FERET (https://www.nist.gov/itl/iad/image-group/color-feret-database), LFW [18] and PaSC [4] datasets.

The rest of this paper will be as follows. Sections 2, 3, 4 and 5 present the related works, the proposed FR methods, the experimental results and the concluding remarks, respectively.

2 Related work

The performance of deep FR can be improved by using advanced training techniques [59, 60]. Chowdhury et al. [9] used a bilinear CNN (B-CNN) to combine outputs of two CNNs, and then the bilinear feature representation is obtained by applying average pooling on these outputs. Hu et al. [15] proposed a two-stream CNN named CNNAuth. Their network is used to monitor the behavioral patterns of users.

Several approaches follow the concept of cropping face patches to train multiple deep networks, and then handling patch representations using a single network [24, 65]. Moreover, multiple networks can be trained by face images with different poses [28] or different viewpoints [21]. Multiple networks can play other roles in addition to classification as they can be used in estimating pose, age, smile and gender of identities [37].

Table 5 Platform specifications

System	Specifications
Type	64-bit Win 10
Processor	Intel Xeon 5670, 12 cores
Graphics Card	NVIDIA GeForce GTX 1070
Installed Memory (RAM)	48G memory

Table 6 Performance of single-region FR using different regions

Dataset	Region	Accuracy	Specificity	Precision	Recall	F_{score}
PaSC	Face	**95.42%**	**95.51%**	**93.73%**	**94.95%**	**94.33%**
	Eyes	93.77%	93.86%	92.16%	93.28%	92.71%
	Nose	94.11%	94.18%	92.41%	93.54%	92.97%
	Mouth	93.93%	94.07%	92.79%	93.89%	93.33%
LFW	Face	**97.94%**	**98.09%**	**96.15%**	**97.33%**	**96.73%**
	Eyes	95.19%	95.26%	93.28%	94.47%	93.87%
	Nose	96.51%	96.58%	94.52%	95.54%	95.02%
	Mouth	95.89%	95.96%	93.87%	95.17%	94.51%
FERET	Face	**97.14%**	**97.23%**	**94.93%**	**96.23%**	**95.57%**
	Eyes	94.87%	94.93%	92.75%	93.67%	93.2%
	Nose	95.24%	95.36%	93.21%	94.34%	93.77%
	Mouth	95.12%	95.25%	93.18%	94.47%	93.82%

Biometric protection techniques [40] that are used for preserving biometric authentication can be categorized to cancelable biometric techniques and biometric cryptosystems. Cancelable biometric techniques adopt the transformation of the original biometric templates using a one-way function. This strategy provides irreversibility, i.e. no information about the original biometric template can be obtained from the transformed one. The concept of cancelability was first introduced using application-dependent parameters to transform biometric samples and compare them with the enrolled protected ones [38].

Most recognition systems that apply cancelable biometrics suffer from degradation in the system performance [40]. To address this problem and obtain remarkable accuracy, multi-biometric template protection techniques were introduced [29, 42]. Multi-biometric schemes perform fusion between different biometric characteristics at the feature level. Data fusion plays a crucial role in multi-biometric recognition systems [22, 43], as it can obtain more consistent, representative and useful information. Furthermore, data fusion can be applied in computer vision tasks, such as object tracking [53–57].

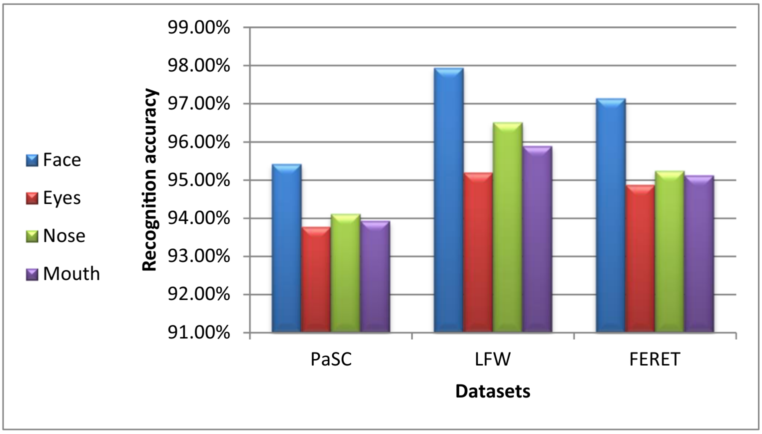

Fig. 4 Comparison between facial regions in terms of recognition accuracy

Table 7 Performance of single-region FR using state-of-the-art CNNs

Dataset	CNN	Accuracy	Specificity	Precision	Recall	F_{score}
PaSC	Arcface [11]	94.85%	94.93%	93.07%	94.18%	93.62%
	Baidu [26]	94.11%	94.22%	92.3%	93.34%	92.81%
	TBE-CNN [12]	95.04%	95.17%	93.28%	94.36%	93.81%
	Ring loss [64]	94.19%	94.27%	92.32%	93.46%	92.88%
	FaceNet [44]	94.69%	94.79%	92.85%	93.96%	93.4%
	DeepVisage [16]	94.47%	94.56%	92.63%	93.75%	93.18%
	DeepID3 [45]	94.35%	94.46%	92.53%	93.65%	93.08%
	Proposed	**95.42%**	**95.51%**	**93.73%**	**94.95%**	**94.33%**
LFW	Arcface [11]	97.48%	97.55%	95.77%	96.96%	96.36%
	Baidu [26]	97.07%	97.15%	95.34%	96.56%	95.94%
	TBE-CNN [12]	97.64%	97.74%	95.93%	97.14%	96.53%
	Ring loss [64]	97.14%	97.27%	95.44%	96.65%	96.04%
	FaceNet [44]	97.45%	97.57%	95.75%	96.91%	96.32%
	DeepVisage [16]	97.33%	97.45%	95.62%	96.84%	96.22%
	DeepID3 [45]	97.26%	97.38%	95.63%	96.83%	96.22%
	Proposed	**97.94%**	**98.09%**	**96.15%**	**97.33%**	**96.73%**
FERET	Arcface [11]	96.61%	96.69%	94.82%	95.94%	95.37%
	Baidu [26]	95.73%	95.82%	93.94%	95.05%	94.49%
	TBE-CNN [12]	96.85%	96.94%	95.16%	96.33%	95.74%
	Ring loss [64]	95.98%	96.11%	94.29%	95.47%	94.87%
	FaceNet [44]	96.44%	96.58%	94.78%	95.93%	95.35%
	DeepVisage [16]	96.27%	96.38%	94.57%	95.76%	95.16%
	DeepID3 [45]	96.15%	96.27%	94.49%	95.62%	95.05%
	Proposed	**97.14%**	**97.23%**	**94.93%**	**96.23%**	**95.57%**

Paul et al. [32] used random projections to perform fusion between face and ear features and principal component analysis (PCA) for DR. In [30], a cancelable template was obtained by mixing continuous and spiral components of different fingerprints. Canuto et al. [5] combined iris and voice data to generate different cancelable transformations. Bloom filters were applied to produce cancelable transformations for iris and face features [13, 41].

3 The proposed FR methods

This work presents three cancelable FR methods that comprise CNNs to extract DFs from facial images, a fusion network to combine features and obtain a final facial descriptor, bioconvolving to provide cancelability of the templates by the ability to change the bioconvolving random masks. The proposed FR methods; region-based, multi-biometric and hybrid-features methods are presented in Figs. 1, 2 and 3, respectively. Each method consists of a number of phases; see Table 1 for more details.

3.1 Convolutional neural networks (CNNs)

CNNs contain several layers, and each layer performs a specific operation on the input images. Table 2 shows a description of the essential rules of a number of CNN layers [16, 19, 25, 50, 61–63]. The proposed CNN model is illustrated in Table 3 with an explanation of the number and size of filters for each layer.

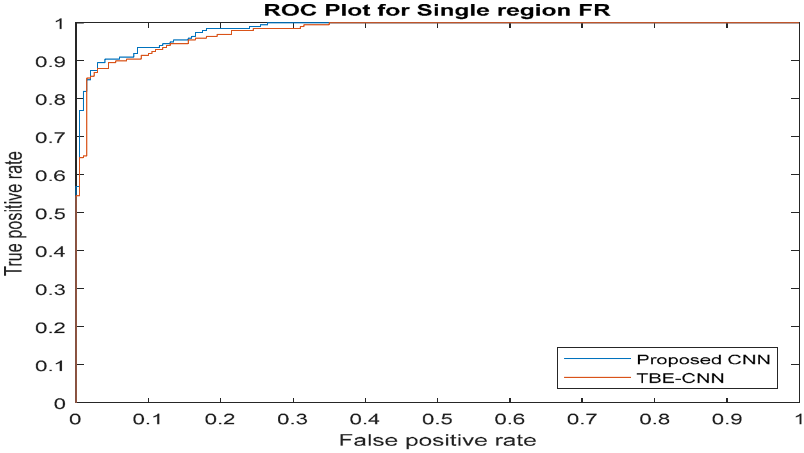

(a)

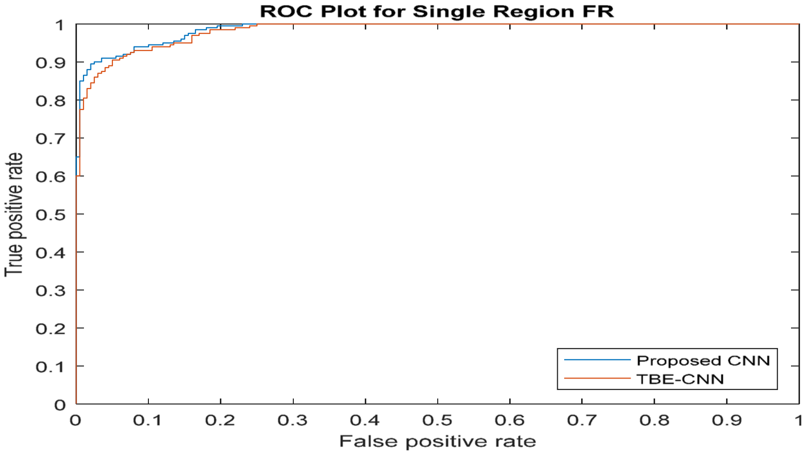

(b)

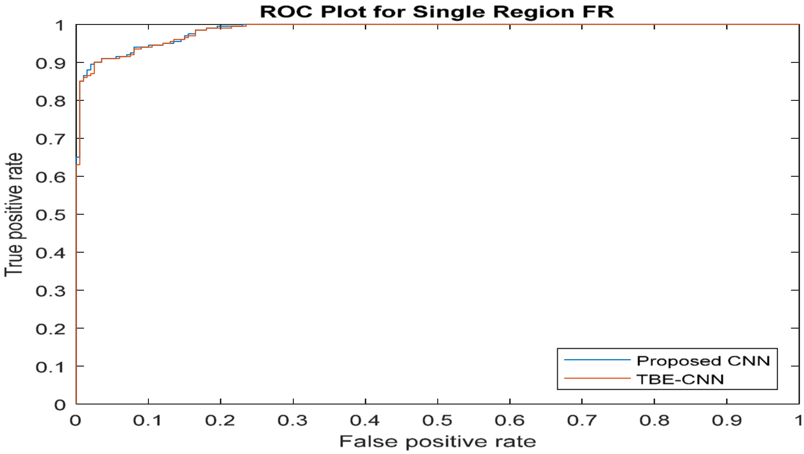

(c)

Fig. 5 ROC plots of single-region FR for (a) PaSC, (b) LFW and (c) FERET datasets

Table 8 Performance of region-based FR using state-of-the-art CNNs

Dataset	CNN	Accuracy	Specificity	Precision	Recall	F_{score}
PaSC	Arcface [11]	97.17%	97.27%	95.66%	96.88%	96.26%
	Baidu [26]	96.28%	96.34%	94.66%	95.87%	95.26%
	TBE-CNN [12]	97.24%	97.33%	95.64%	96.91%	96.27%
	Ring loss [64]	96.54%	96.62%	94.98%	96.14%	95.55%
	FaceNet [44]	96.76%	96.82%	95.22%	96.44%	95.82%
	DeepVisage [16]	96.68%	96.75%	95.04%	96.25%	95.64%
	DeepID3 [45]	96.51%	96.57%	94.95%	96.18%	95.56%
	Proposed	**97.38%**	**97.48%**	**95.89%**	**97.12%**	**96.5%**
LFW	Arcface [11]	98.66%	98.74%	97.14%	98.25%	97.69%
	Baidu [26]	97.89%	97.98%	96.38%	97.56%	96.96%
	TBE-CNN [12]	98.71%	98.8%	97.22%	98.38%	97.79%
	Ring loss [64]	98.13%	98.22%	96.56%	97.78%	97.16%
	FaceNet [44]	98.39%	98.47%	96.86%	98.08%	97.46%
	DeepVisage [16]	98.26%	98.33%	96.74%	97.84%	97.28%
	DeepID3 [45]	98.19%	98.28%	96.63%	97.87%	97.24%
	Proposed	**98.93%**	**99.08%**	**97.51%**	**98.77%**	**98.13%**
FERET	Arcface [11]	98.52%	98.63%	96.82%	98.14%	97.47%
	Baidu [26]	97.61%	97.69%	95.91%	97.12%	96.51%
	TBE-CNN [12]	98.68%	98.75%	97.03%	98.26%	97.64%
	Ring loss [64]	97.76%	97.87%	96.18%	97.38%	96.77%
	FaceNet [44]	98.14%	98.25%	96.55%	97.76%	97.15%
	DeepVisage [16]	97.97%	98.09%	96.39%	97.53%	96.95%
	DeepID3 [45]	97.81%	97.92%	96.16%	97.38%	96.76%
	Proposed	**98.89%**	**99.02%**	**97.21%**	**98.48%**	**97.84%**

3.2 Fusion network

This network consists of two layers: a local layer, which consists of a number of parallel CNNs, and a fusion layer, which is used to form the final descriptor that can be computed as:

$$\mathbf{y}' = \sum_{i=1}^{N} \mathbf{W}_{\mathbf{f}}^{(i)} \mathbf{F}^{(i)}(.) + \mathbf{b}_{\mathbf{f}}^{(i)} \tag{5}$$

where $\mathbf{y}'$ is the final facial descriptor, N is the number of parallel CNNs, $\mathbf{W}_{\mathbf{f}}^{(i)}$ and $\mathbf{b}_{\mathbf{f}}^{(i)}$ are the corresponding weights and bias of a particular CNN (i), and $\mathbf{F}^{(i)}(.)$ is the deep feature vector extracted from a CNN (Fig. 3).

3.3 Bioconvolving method

This method incorporates a convolution operation to generate cancelable biometric templates [31]. In bioconvolving, each original sequence, $r(n)$, $n = 1, \ldots, F$, has a transformed sequence $f(n)$, $n = 1, \ldots, F$, which represents the original biometric template in an encrypted form. We have $\mathbf{d}=[d_0, \ldots, d_w]^T$. It is clear that the vector $\mathbf{d}$ is the key of the transformation. The original sequence $r(n)$ is convolved with $d(n)$. The transformed sequence can be computed as:

$$f(n) = r(n) * d(n) \tag{6}$$

From the original biometric templates, we can generate different templates by simply changing the values of $\mathbf{d}$.

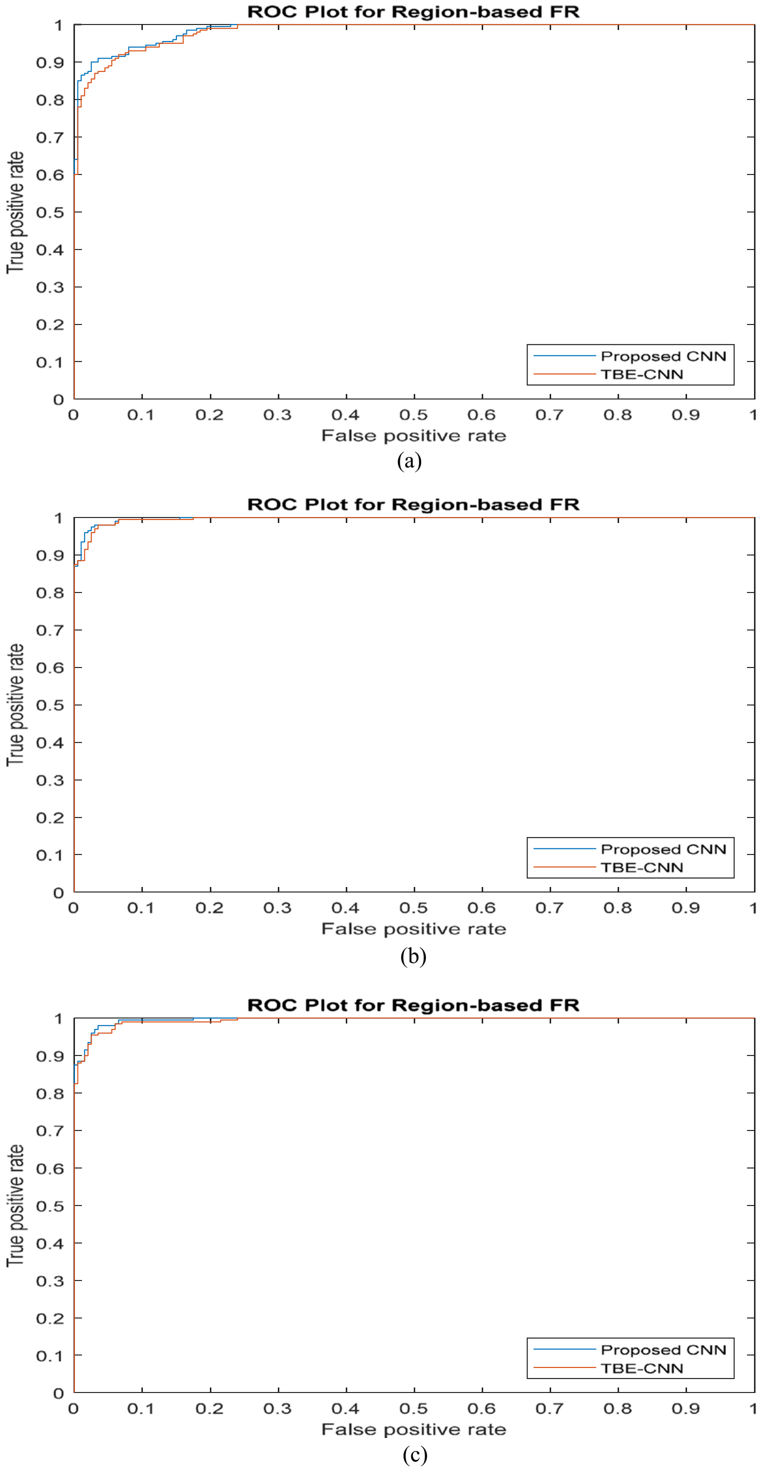

Fig. 6 ROC plots of region-based FR for (a) PaSC, (b) LFW and (c) FERET datasets

Table 9 Experimental results of single-biometric FR

Biometric	Accuracy	Specificity	Precision	Recall	F_{score}
Face	97.14%	97.23%	94.93%	96.23%	95.57%
Iris [7]	94.9%	95.06%	92.98%	93.87%	93.42%
Palm Print [10]	94.85%	94.96%	92.74%	93.94%	93.33%
Fingerprint [6]	96.13%	96.27%	94.41%	95.5%	94.95%
Ear [3]	97.97%	98.08%	96.3%	97.29%	96.79%

4 Experimental results

This section reveals the effectiveness of several FR methods in terms of the performance metrics presented in Table 4. Furthermore, comparisons with the state-of-the-art methods are provided to demonstrate the superiority of the proposed methods. Table 5 shows the specifications of the platform that is used for experiments. Stochastic gradient descent algorithm is exploited for CNN training and L_2 regularization is applied (weight decay = 5×10^4). The learning rate is set to 0.1 at the beginning of the CNN training. The training is stopped after 5 epochs [16].

4.1 Evaluation of single-region FR

In single-region FR, a single CNN extracts features from a single facial region; face, nose, eyes or mouth. To demonstrate the most effective region in face images, Table 6 presents the experimental results of single-region FR using various facial regions. These regions are detected from the original images as mentioned in section 3.

From Table 6, it is clear that the face region achieves better performance than those of the other regions. Moreover, the nose region gives good results as it is less affected by changes in positions and expressions compared with eyes and mouth regions. Figure 4 depicts a comparison between facial regions for various datasets in terms of recognition accuracy.

Based on the obtained results, single-region FR depends on the selected face regions. Table 7 gives the comparison results of the state-of-the-art CNNs for single-region FR.

The results in Table 7 indicate that the performance of single-region FR is enhanced using the proposed CNN model. The above-mentioned results and the receiver operating characteristic (ROC) plots shown in Fig. 5 confirm the superiority of the proposed CNN model.

Table 10 Performance of multi-biometric FR using the state-of-the-art CNNs

CNN	Accuracy	Specificity	Precision	Recall	F_{score}
Arcface [11]	98.37%	98.44%	96.68%	97.98%	97.32%
Baidu [26]	97.26%	97.37%	95.67%	96.86%	96.26%
TBE-CNN [12]	98.19%	98.29%	96.58%	97.74%	97.15%
Ring loss [64]	97.13%	97.27%	95.41%	96.71%	96.05%
FaceNet [44]	97.94%	98.06%	96.36%	97.54%	96.94%
DeepVisage [16]	97.7%	97.89%	95.43%	96.71%	96.06%
DeepID3 [45]	97.54%	97.63%	95.83%	96.91%	96.36%
Proposed	**98.77%**	**98.89%**	**96.73%**	**98.23%**	**97.47%**

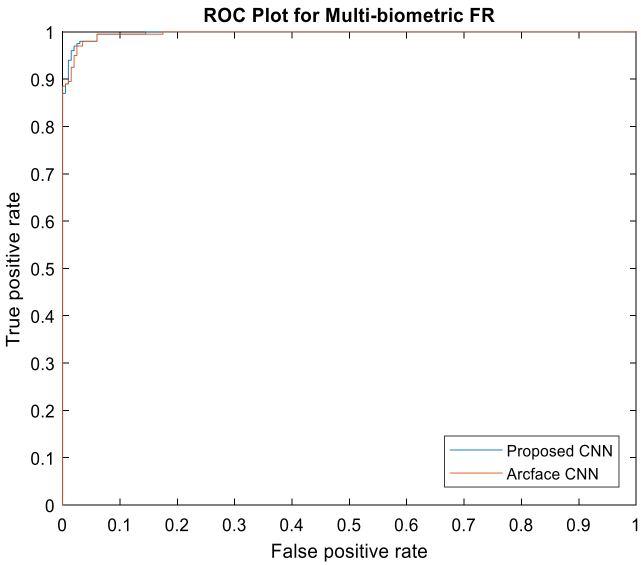

Fig. 7 ROC plots of multi-biometric FR

4.2 Evaluation of region-based FR

Region-based FR incorporates the use of different facial regions to train multiple CNNs of the same architecture. Table 8 provides the experimental results of region-based FR using various CNN models.

We can observe from Table 8 that the region-based FR using the proposed CNN model outperforms TBE-CNN and Arcface models for different datasets. ROC plots are introduced in Fig. 6.

4.3 Evaluation of multi-biometric FR

This method uses different biometric traits to train multiple CNNs. Tables 9 presents the experimental results of single-biometric FR, where a single biometric is used to train a single

Table 11 Performance of hybrid-features FR using different FE and DR methods on FERET dataset

FE Algorithm	DR Method	Accuracy	Specificity	Precision	Recall	F_{score}
SURF	*PCA*	93.35%	93.43%	91.44%	92.32%	91.87%
SIFT		93.53%	93.59%	91.62%	92.57%	92.09%
LBP		94.56%	94.67%	92.77%	93.82%	93.29%
ORB		93.91%	93.98%	92.09%	93.15%	92.61%
HOG		95.26%	95.37%	93.46%	94.55%	94%
SURF	*ICA*	95.58%	95.66%	93.75%	94.84%	94.29%
SIFT		96.22%	96.34%	94.42%	95.61%	95.01%
LBP		97.14%	97.25%	95.31%	96.48%	95.89%
ORB		96.87%	96.98%	95.19%	96.33%	95.75%
HOG		**97.89%**	**97.97%**	**96.11%**	**97.27%**	**96.68%**

Table 12 Performance of hybrid-features FR using different FE and DR methods on LFW dataset

FE Algorithm	DR Method	Accuracy	Specificity	Precision	Recall	F_{score}
SURF	*PCA*	95.28%	95.39%	93.51%	94.36%	93.93%
SIFT		96.13%	96.28%	94.48%	95.27%	94.87%
LBP		96.74%	96.88%	95.11%	96.13%	95.61%
ORB		96.48%	96.55%	94.83%	95.77%	95.29%
HOG		96.95%	97.08%	95.36%	96.34%	95.84%
SURF	*ICA*	96.93%	97.02%	95.13%	96.15%	95.63%
SIFT		97.15%	97.27%	95.42%	96.39%	95.9%
LBP		97.72%	97.84%	95.95%	96.74%	96.34%
ORB		97.69%	97.76%	95.96%	96.79%	96.37%
HOG		**98.64%**	**98.79%**	**96.98%**	**97.85%**	**97.41%**

Table 13 Performance of hybrid-features FR using different FE and DR methods on PaSC dataset

FE Algorithm	DR Method	Accuracy	Specificity	Precision	Recall	F_{score}
SURF	*PCA*	93.14%	93.23%	91.34%	92.34%	91.83%
SIFT		94.23%	94.36%	92.45%	93.53%	92.98%
LBP		94.76%	94.85%	92.97%	93.83%	93.39%
ORB		94.57%	94.66%	92.75%	93.81%	93.27%
HOG		95.07%	95.15%	93.22%	94.26%	93.73%
SURF	*ICA*	95.04%	95.12%	93.15%	94.22%	93.68%
SIFT		95.3%	95.41%	93.43%	94.51%	93.96%
LBP		96%	96.11%	94.16%	95.26%	94.7%
ORB		95.83%	95.92%	93.95%	95.06%	94.5%
HOG		**96.69%**	**96.77%**	**94.88%**	**95.94%**	**95.4%**

Table 14 Performance of hybrid-features FR using the state-of-the-art CNNs

Dataset	CNN	Accuracy	Specificity	Precision	Recall	F_{score}
PaSC	Arcface [11]	96.58%	96.67%	94.33%	95.41%	94.86%
	Baidu [26]	95.39%	95.46%	93.5%	94.66%	94.07%
	TBE-CNN [12]	96.25%	96.34%	94.47%	95.56%	95.01%
	Ring loss [64]	95.56%	95.64%	93.77%	94.83%	94.29%
	FaceNet [44]	95.93%	96.03%	94.23%	95.24%	94.73%
	DeepVisage [16]	95.87%	95.97%	94.09%	95.14%	94.61%
	DeepID3 [45]	95.71%	95.8%	93.84%	94.92%	94.37%
	Proposed	**96.69%**	**96.77%**	**94.88%**	**95.94%**	**95.4%**
LFW	Arcface [11]	98.54%	98.65%	97.13%	98.03%	97.57%
	Baidu [26]	96.73%	96.83%	95.05%	96.12%	95.58%
	TBE-CNN [12]	98.13%	98.25%	96.56%	97.58%	97.06%
	Ring loss [64]	96.86%	96.97%	95.28%	96.23%	95.75%
	FaceNet [44]	97.28%	97.39%	95.61%	96.76%	96.18%
	DeepVisage [16]	97%	97.14%	95.46%	96.48%	95.96%
	DeepID3 [45]	96.93%	97.09%	95.37%	96.44%	95.9%
	Proposed	**98.64%**	**98.79%**	**96.98%**	**97.85%**	**97.41%**
FERET	Arcface [11]	96.54%	96.68%	94.89%	95.93%	95.4%
	Baidu [26]	95.13%	95.24%	93.41%	94.55%	93.97%
	TBE-CNN [12]	96.93%	97.08%	95.27%	96.31%	95.78%
	Ring loss [64]	95.37%	95.45%	93.68%	94.77%	94.22%
	FaceNet [44]	96.23%	96.3%	94.43%	95.53%	94.97%
	DeepVisage [16]	95.78%	95.89%	94.17%	95.16%	94.66%
	DeepID3 [45]	95.69%	95.78%	93.95%	95.13%	94.53%
	Proposed	**97.89%**	**97.97%**	**96.11%**	**97.27%**	**96.68%**

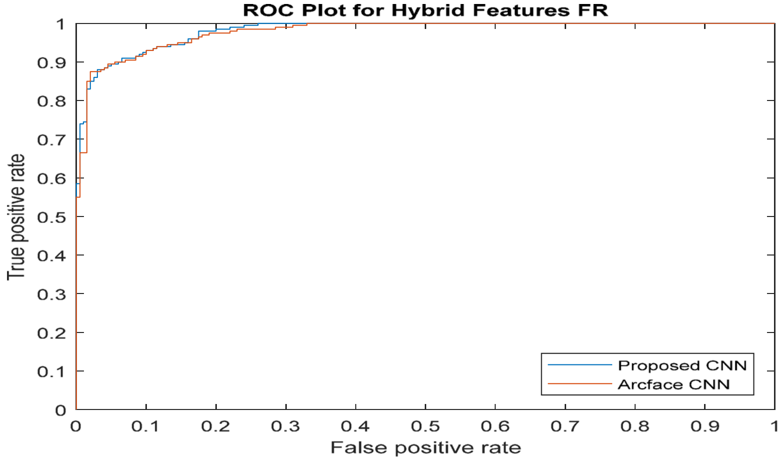

(a)

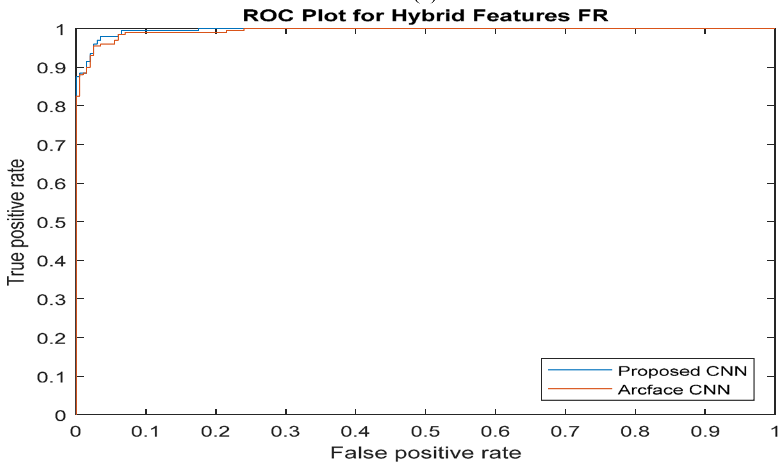

(b)

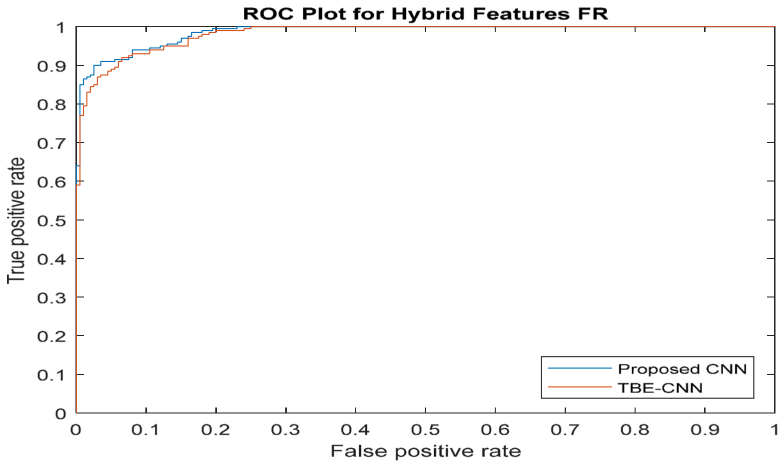

(c)

Fig. 8 ROC plots of hybrid-features FR for (a) PaSC, (b) LFW and (c) FERET datasets

Table 15 Effect of cancelable methods on recognition accuracy

FR methods	Without Cancelability	Bioconvolving	Bloom Filter [23]
Single region	97.92%	97.14%	93.18%
Region-based	99.83%	98.89%	93.93%
Multi-biometric	99.65%	98.77%	93.86%
Hybrid-features	98.54%	97.89%	93.31%

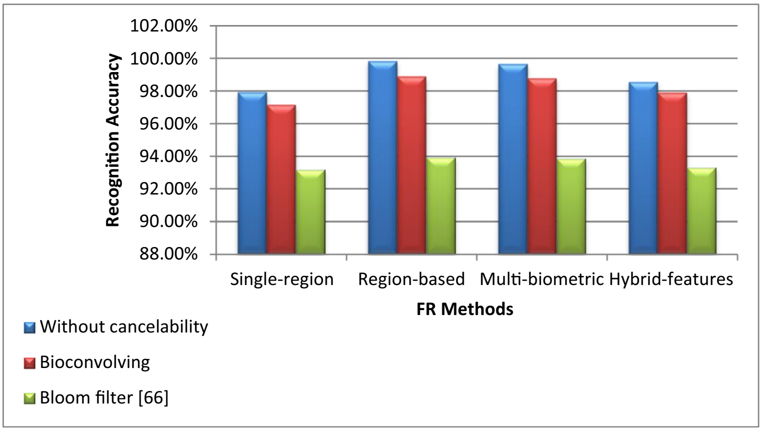

Fig. 9 Effect of different cancelable biometric recognition methods on recognition accuracy

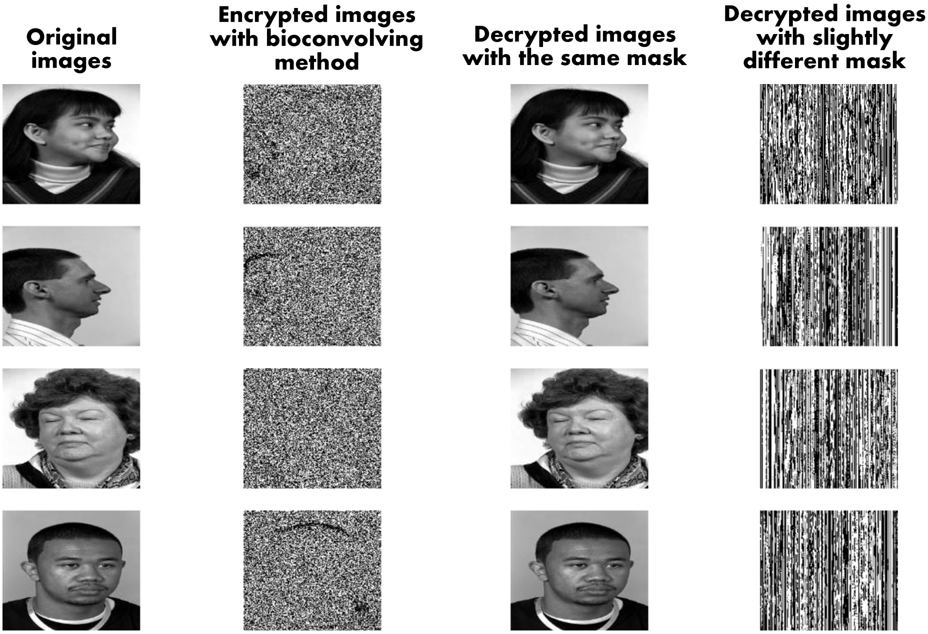

Fig. 10 Encryption and decryption of a class of face images with the same mask and a slightly-different mask

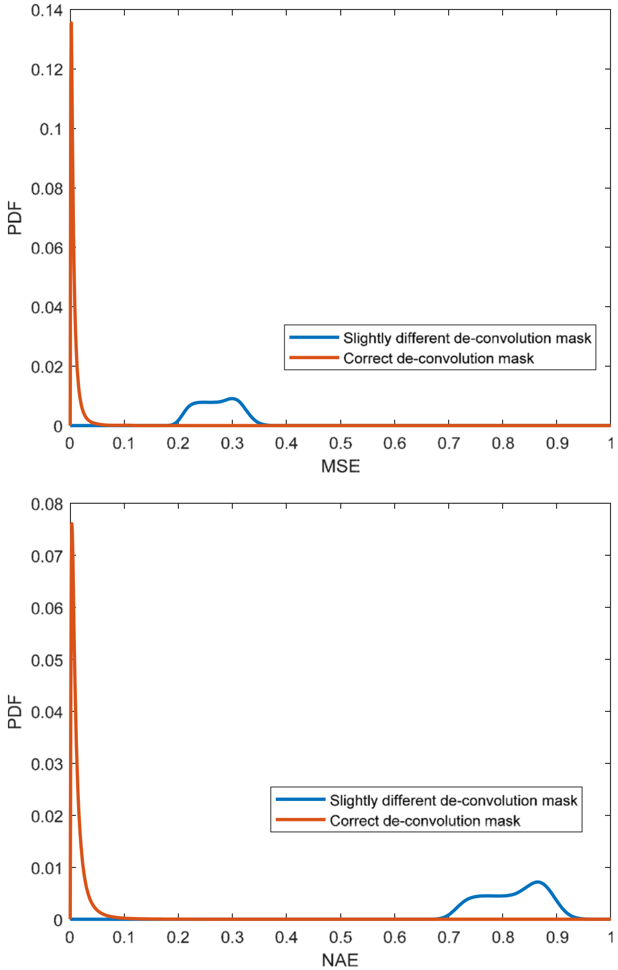

Fig. 11 The PDFs of the MSE and the NAE for the correct and slightly different de-convolution mask outputs

CNN. Table 10 shows the results of the proposed multi-biometric FR using the state-of-the-art CNNs.

From Tables 9 and 10, we can say that the proposed CNN model contributes to improving the FR performance. The recognition accuracy using the proposed model reaches (98.77%), which is larger than that of the Arcface (98.37%). The ROC plots in Fig. 7 confirm these findings. As well, it is clear that the proposed multi-biometric method gives better results than those of the single-biometric one.

4.4 Evaluation of hybrid-features FR

The performance of the hybrid-features FR is illustrated in Tables 11, 12 and 13 using the proposed CNN model to extract DFs, different feature extraction (FE) algorithms (SIFT [47], SURF [8], LBP [33], ORB [51] or HOG [2]) to obtain hand-crafted features, PCA [58] or ICA [46] for DR, and a fusion network for feature combination.

It can be noticed from Tables 11, 12 and 13 that the HOG algorithm for FE and the ICA for DR give remarkable results. For more validation of the effectiveness of the proposed CNN, Table 14 illustrates the performance of hybrid-features FR using the state-of-the-art CNNs.

Table 14 confirms the improvement in hybrid-features FR. The proposed model is superior to the state-of-the-art CNNs as depicted in Fig. 8.

4.5 Evaluation of the proposed cancelable biometrics approach

The proposed approach adopts bioconvolving to provide user privacy. This results in a slight degradation in system performance. Table 15 introduces the values of recognition accuracy of the proposed methods under different conditions; without cancelability, with bioconvolving, and with bloom filter [23].

From Table 6, it can be observed that bioconvolving performs better than bloom filter. The degradation in recognition accuracy is 0.78% for single-region FR, 0.94% for region-based FR, 0.88% for multi-biometric FR and 0.65% for hybrid-features FR; see Fig. 9.

To verify the security of the proposed methods and evaluate the ability and strength of bioconvolving in protecting data, Fig. 10 illustrates encryption and decryption of a class of face images with the same mask and with a slightly different mask.

It is clear from Fig. 10 that a slight change in the mask leads to totally different outputs from the original faces, which ensures the strength of the proposed bioconvolving algorithm. To perform a statistical analysis of bioconvolving, the mean square error (MSE) and normalized absolute error (NAE) between original images and deconvolution outputs are studied with correct and slightly different deconvolution masks. Figure 11 reveals the probability density functions (PDFs) of these metrics.

From Fig. 11, it can be noticed that incorrect deconvolution leads to totally different images from the original ones.

From all previous results, it is clear that the fusion leads to more useful and robust facial descriptors. This results in the superiority of the region-based, multi-biometric and hybrid-features methods to the single-region FR method. Also, region-based FR achieves the best results due to the use of different facial regions which can achieve good performance in the presence of occlusions. On the other hand, region-based and multi-biometric FR methods are more complex than single-region FR method due to the use of multiple CNNs.

5 Conclusions

This paper discussed the performance of single-region, region-based, multi-biometric and hybrid-features FR methods. The proposed methods adopt extraction of deep features using CNNs, combining features by a fusion network, and cancelability to provide privacy and security of user templates. A new CNN model was proposed. The experimental results on challenging datasets demonstrated that the proposed CNN model outperforms the state-of-the-art CNNs, fusion-based methods performed better than single-region method, region-based FR achieves a promising performance in the presence of occlusions, and applying bioconvolving method results in adding security and privacy with a slight degradation in the recognition accuracy.

Compliance with ethical standards

Conflict of interest The authors declare that they have no conflict of interest.

Ethical approval All procedures performed in studies involving human participants were in accordance with the ethical standards of the institutional and/or national research committee and with the 1964 Helsinki declaration and its later amendments or comparable ethical standards.

Informed consent Informed consent was obtained from all individual participants included in the study.

References

1. Agrawal A, Mittal N (2019) Using CNN for facial expression recognition: a study of the effects of kernel size and number of filters on accuracy. Visual Comput J: 1–8
2. Ali H, Jahangir U, Yousuf B, Noor A (2017) Human action recognition using SIFT and HOG method. International Conference on Information and Communication Technologies (ICICT): 6–10
3. AMI ear database (2018) http://ctim.ulpgc.es/research_works/ami_ear_database/ Accessed November
4. Beveridge J, Phillips J, Bolme D, Draper B, Givens G, Lui Y, Teli M, Zhang H, Scruggs W, Bowyer K (2013) The challenge of face recognition from digital point-and-shoot cameras. IEEE Int Conf Biometrics, Theory, Appl Syst: 1–8
5. Canuto A, Pintro F, Xavier-Junior J (2013) Investigation fusion approaches in multi-biometric cancellable recognition. ESA 40:1971–1980
6. CASIA Fingerprint Image Database Version 5.0 (2018) http://biometrics.idealtest.org/dbDetailForUser.do?id=7 Accessed November
7. CASIA-IrisV3 Database (2018) http://www.cbsr.ia.ac.cn/english/IrisDatabase.asp. Accessed May
8. Cheng C, Wang X, Li X (2017) UAV image matching based on surf feature and harris corner algorithm. International Conference on Smart and Sustainable City (ICSSC): 1–6
9. Chowdhury A, Lin T, Maji S, Learned-Miller E (2016) One-tomany face recognition with bilinear cnns. WACV: 1–9
10. COEP Palm Print Database (2018) http://www.coep.org.in/resources/coeppalmprintdatabase.m Accessed December
11. Deng J, Guo J, Zafeiriou S (2018) Arcface: additive angular margin loss for deep face recognition. arXiv preprint arXiv:1801.07698
12. Ding C, Tao D (2017) Trunk-branch ensemble convolutional neural networks for video-based face recognition. IEEE Trans Pattern Anal Mach Intell
13. Gomez-Barrero M, Rathgeb C (2014) Protected facial biometric templates based on local gabor patterns and adaptive bloom filters. ICPR: 4483–4488
14. Hai H, Hao Z, Xu Y, Lu Z, Lu Q, Ai-Yun Z (2019) Faster R-CNN for marine organisms detection and recognition using data augmentation. Neurocomputing: 1–13
15. Hailong H, Yantao L, Zhangqian Z, Gang Z (2019) CNNAuth: continuous authentication via two-stream convolutional neural networks. IEEE NAS
16. Hasnat A, Bohn'e J, Milgram J, Gentric S, Chen L (2017) DeepVisage: making face recognition simple yet with powerful generalization skills. CVPR: 1–12
17. He X, Yan S, Hu Y, Niyogi P, Zhang J (2005) Face recognition using laplacian faces. IEEE Trans Pattern Anal Mach Intell 3:328–340
18. Huang G, Ramesh M, Berg T, Learned-Miller E (2007) Labeled faces in the wild: a database for studying face recognition in unconstrained environments. Technical report. University of Massachusetts, Amherst, pp 07–49
19. Ioffe S, Szegedy CH (2015) Batch normalization: accelerating deep network training by reducing internal covariate shift. arXiv: 1502.03167v3 [cs.LG]: 1–11
20. Junaid B, Maheen B, Kafil U, Waheed N, Varsha D, Abdul S (2019) Facial expression recognition and analysis of interclass false positives using CNN. Future of Information and Communication Conference: 46–54
21. Kan M, Shan S, Chen X (2016) Multi-view deep network for cross-view classification. CVPR: 4847–4855
22. Kelkboom E, Zhou X (2009) Multi-algorithm fusion with template protection. BTAS:1–7
23. Lin Y, Xun L (2018) A cancelable multi-biometric template generation algorithm based on bloom filter. International Conference on Algorithms and Architectures for Parallel Processing: 547–559

24. Liu J, Deng Y, Bai T, Wei Z, Huang C (2015) Targeting ultimate accuracy: face recognition via deep embedding. arXiv preprint arXiv:1506.07310
25. Liu W, Jia Y, Sermanet P, Rabinovich A (2015) Going deeper with convolutions. IEEE conference on computer vision and pattern recognition: 1–9
26. Liu J, Deng Y, Huang C (2015) Targeting ultimate accuracy: face recognition via deep embedding. arXiv: 1506.07310
27. Marco C, Oscar D, Cayetano G, Mario H (2007) ENCARA2: real-time detection of multiple faces at different resolutions in video streams. J Vis Commun Image Represent 18(2):130–140
28. Masi I, Rawls S, Medioni G, Natarajan P (2016) Pose-aware face recognition in the wild. CVPR: 4838–4846
29. Nagar A, Nandakumar K, Jain A (2012) Multibiometric cryptosystems based on feature-level fusion. IEEE TIFS 7(1):255–268
30. Othman A, Ross A (2013) On mixing fingerprints. IEEE TIFS 8(1):260–267
31. Patel V, Ratha N, Chellappa R (2015) Cancelable biometrics [a review]. IEEE Signal Process Mag, 54–65
32. Paul P, Gavrilova M (2012) Multimodal cancelable biometrics. ICCI*CC: 43–49
33. Pei S, Chen M, Yu Y, Tang S, Zhong C (2017) Compact LBP and WLBP descriptor with magnitude and direction difference for face recognition. IEEE International Conference on Image Processing (ICIP): 1067–1071
34. Polash P, Gavrilova M, Klimenko S (2014) Situation awareness of cancelable biometric system. Visual Comput J 30:1059–1067
35. Priya T, Sarika J, Durgesh K (2018) Person-dependent face recognition using histogram of oriented gradients (HOG) and convolution neural network (CNN). International Conference on Advanced Computing Networking and Informatics: 35–40
36. Rajeev R, Vishal M, Rama C (2019) HyperFace: a deep multi-task learning framework for face detection, landmark localization, pose estimation, and gender recognition. IEEE Trans Pattern Anal Mach Intell 41(1): 121–135
37. Ranjan R, Sank S, Castillo C, Chellappa R (2017) An all-in-one convolutional neural network for face analysis. FG IEEE: 17–24
38. Ratha N, Connell J, Bolle R (2001) Enhancing security and privacy in biometrics-based authentication systems. IBM SJ 40:614–634
39. Ratha N, Chikkerur S, Connell J, Bolle R (2007) Generating cancelable fingerprint templates. IEEE Trans Pattern Anal Mach Intell 29:561–572
40. Rathgeb C, Uhl A (2011) A survey on biometric cryptosystems and cancelable biometrics. EURASIP JIS 3(3)
41. Rathgeb C, Breitinger F, Busch C (2013) Alignment-free cancelable iris biometric templates based on adaptive bloom filters. ICB: 1–8
42. Ross A, Jain A (2003) Information fusion in biometrics. PRL 24(13):2115–2125
43. Ross A, Nandakumar K, Jain A (2006) Handbook of multi-biometrics, Springer-Verlag
44. Schroff F, Kalenichenko D, Philbin J (2015) Facenet: a unified embedding for face recognition and clustering. CVPR:815–823
45. Sun Y, Liang D, Wang X, Tang X (2015) DeepID3: Face recognition with very deep neural networks arXiv: 1502.00873
46. Swathi K, Kalyana V, Quek CH (2018) Evolutionary based ICA with reference for EEGμRhythm extraction. IEEE Access: 19702 – 19713
47. Sylvia W, Kamalaharidharini T (2017) Robust face recognition and classification system based on SIFT and DCP techniques in image processing. International Conference on Intelligent Computing and Control (I2C2): 1–8
48. Taigman Y, Yang M, Ranzato M, Wolf L (2014) Deepface: closing the gap to human-level performance in face verification. CVPR: 1701–1708
49. Teoh A, Goh A, Ngo D (2006) Random multispace quantization as an analytic mechanism for biohashing of biometric and random identity inputs. IEEE Trans Pattern Anal Mach Intell 28:1892–1901
50. Theodoridis S, Koutroumbas K (2008) Pattern recognition. Fourth edition. Academic Press, 4th edition
51. Vinay A, Kumar C, Shenoy R (2015) ORB-PCA based feature extraction technique for face recognition. Second International Symposium on Computer Vision and the Internet: 614–621
52. Wright J, Yang A, Ganesh A, Sastry S, Ma Y (2009) Robust face recognition via sparse representation. IEEE Trans Pattern Anal Machine Intell 2:210–227
53. Xiangyuan L, Ma A, Pong Y, Rama C (2015) Joint sparse representation and robust feature-level fusion for multi-Cue visual tracking. IEEE Trans Image Process 24(12):5826–5841
54. Xiangyuan L, Shengping Z, Pong Y (2016) Robust joint discriminative feature learning for visual tracking. Twenty-fifth international joint conference on artificial Intelligence: 3403–3410
55. Xiangyuan L, Mang Y, Shengping Z, Pong Y (2018) Robust collaborative discriminative learning for RGB-infrared tracking. The thirty-second AAAI conference on artificial Intelligence: 7008–7015

56. Xiangyuan L, Shengping Z, Pong Y, Rama C (2018) Learning common and feature-specific patterns: a novel multiple-sparse-representation-based tracker. IEEE Trans Image Process 27(4):2022–2037
57. Xiangyuan L, Mang Y, Rui Sh, Bineng Zh, Pong Y, Huiyu Z (2019) Learning modality-consistency feature templates: a robust RGB-infrared tracking system. IEEE Trans Industrial Electronics
58. Xiaolin X, Yicong Z (2018) Two-dimensional quaternion PCA and sparse PCA. IEEE Transactions on Neural Networks and Learning Systems: 1–15
59. Xin Q, Gang Z, Yantao L, Ge P (2012) RadioSense: Exploiting Wireless Communication Patterns for Body Sensor Network Activity Recognition. IEEE 33rd Real-Time Systems Symposium
60. Xin Q, Matthew K, Gang Z, Yantao L, Zhen R (2013) AdaSense: adapting sampling rates for activity recognition in body sensor networks. IEEE RTAS
61. Yakopcic C, Alom M, Taha T (2017) Extremely parallel memristor crossbar architecture for convolutionalneural network implementation. International Joint Conference on Neural Networks (IJCNN): 1696–1703
62. Yuan Z, Liu Y, Yue J, Li J, Yang H (2017) CORAL: Coarse-grained reconfigurable architecture for Convolutional Neural Networks. IEEE/ACM International Symposium on Low Power Electronics and Design (ISLPED): 1–6
63. Zhang X, Ren Sh, Sun J (2016) Deep residual learning for image recognition. IEEE conference on computer vision and pattern recognition: 770–778
64. Zheng Y, Pal D, Savvides M (2018) Ring loss: convex feature normalization for face recognition. CVPR
65. Zhou E, Cao Z, Yin Q (2015) Naive-deep face recognition: touching the limit of lfw benchmark or not? arXiv preprint arXiv:1501.04690

Essam Abdellatef received the Master degree in Electronics and Communications Engineering from the Faculty of Engineering, Mansoura University, Egypt by 2015. Currently he is pursuing his PhD Degree in Menoufia University-Egypt. He is now an assistant lecturer at the electronics and communications engineering department, Delta Higher Institute for Engineering and Technology-Egypt. His main research area includes Deep Learning applications, 3D object reconstruction and image processing.

Nabil A. Ismail was the Dean of the Faculty of Computers and Information, Menoufia University, (Aug. 2006-Aug.2008). He is now a Professor of Computer Science and Engineering, Faculty of Electronic Engineering, Menoufia University. Prof. Ismail obtained his PhD degree in Computer Eng. from Durham University, England, in 1983. His main research area includes Deep Learning applications and computer vision, Tomography, Computer security, Computer architecture, Elliptic curve cryptography, Processor design, Light-power smart devices, Security applications, EIT algorithms, and Multi-core/many-core parallel programming.

Salah S. E. Abd Elrahman received the B. Sc. degree in Industrial Electronics Engineering May 1988, from the Faculty of Electronic Engineering, Menouf, Menoufia University, Egypt. He received the M. Sc. degree in Computer Science and Engineering 9th of July 1994, from the Faculty of Electronic Engineering, Menouf, Menoufia University, Egypt. The thesis subject was "A Design of an Arabic Programming Language and its Compiler." He obtained his Ph. D. degree in Computations 11th of July 2003, from the Dept. of Computation, University of Manchester Institution of Science and Technology (UMIST), U. K. The thesis subject was "Object-Oriented Technology for System-Level Design." His main research area is developing Computer Systems that includes Embedded Systems, Real-Time Systems, Concurrent Systems, and Software Systems such as compilers.

Khalid N. Ismail is an Assistant professor at the Faculty of Computers and Information, Menoufia University, Egypt. He is also a research associate at the Department of Computer Science, Durham University, UK. He has been working as an academic research fellow at Nottingham, Bath and Leeds Universities. He obtained his PhD from University of Leeds, UK, in 2013. His research interests include advanced computer vision and image processing, 3D image reconstruction, tomography and deep machine learning applied to complex real world problems.

Mohamed Rihan received his B.Sc. in electronics and communication engineering, with honors from Menoufia University, Egypt. He received his M.Sc. and PhD in electronics and communication engineering from Egypt-Japan University of Science and Technology in 2012 and 2015 respectively. Currently, he is a postdoctoral research fellow with College of Information Engineering, Shenzhen University, China. He is also serving as an assistant professor at the Faculty of Electronic Engineering (FEE), Menoufia University, Egypt. His research interests include massive MIMO and mmWave communications, interference alignment, resource allocation, and cognitive heterogeneous networks.

Fathi E. Abd El-Samie received the B.Sc. (Honors), M.Sc., and Ph.D. from the Faculty of Electronic Engineering, Menoufia University, Menouf, Egypt, in 1998, 2001, and 2005, respectively. He has received the most cited paper award from Digital Signal Processing journal for 2008. His current research areas of interest include image enhancement, image restoration, image interpolation, super resolution reconstruction of images, data hiding, multimedia communications, medical image processing, optical signal processing, and digital communications.

Affiliations

Essam Abdellatef[1] · Nabil A. Ismail[2] · Salah Eldin S. E. Abd Elrahman[2] · Khalid N. Ismail[3,4] · Mohamed Rihan[5] · Fathi E. Abd El-Samie[5]

Nabil A. Ismail
Nabil.Ismail@el-eng.menofia.edu.eg

Salah Eldin S. E. Abd Elrahman
salaheldeen@el-eng.menofia.edu.eg

Khalid N. Ismail
Khalid.n.ismail@gmail.com

Mohamed Rihan
mohamed.elmelegy@el-eng.menofia.edu.eg

Fathi E. Abd El-Samie
fathi_sayed@yahoo.com

1 Electronics and Communication Department, Delta Academy for Engineering, Mansoura, Egypt

2 Department of Computer Science and Engineering, Faculty of Electronic Engineering, Menoufia University, Menoufia 32952, Egypt

3 Department of Computer Science, Durham University, Durham DH1 3LE, UK

4 Information Technology Department, Faculty of Computers and Information, Menoufia University, Menoufia, Egypt

5 Department of Electronics and Electrical Communications Engineering, Faculty of Electronic Engineering, Menoufia University, Menoufia 32952, Egypt